Journal of Institute of Science and Technology, 31(1), 75-78 (2026)
ISSN: 2467-9062 (print), e-ISSN: 2467-9240
https://dog.org/10.3126/jist.v31i1.91344

Research Article

Ab INITIO STUDY OF Hf_2InN MAX PHASE: STRUCTURAL, MECHANICAL, DYNAMICAL, ELECTRONIC, MAGNETIC, AND OPTICAL INSIGHTS

Sushil Shrestha[1], Suraj Timalsina[1], Bibek Dhital[1], Dipesh Dhital[2], Ganesh Paudel[2], Om Shree Rijal[1,2], Hari Krishna Neupane[1,2*]

[1]*Central Department of Physics, Institute of Science and Technology, Tribhuvan University, Kathmandu Nepal*
[2]*Amrit Campus, Institute of Science and Technology, Tribhuvan University, Kathmandu Nepal*
**Correspondence: hari.neupane@ac.tu.edu.np*

*(**Received:** March 18, 2026; **Revised:** April 20, 2026; **Accepted:** May 12, 2026)*

ABSTRACT

As MAX phase compounds combine the properties of metal and ceramics, they can be used in a variety of applications. In this work, we explored the structural, mechanical, dynamical, electronic, magnetic, and optical properties of the Hf_2InN MAX phase compound using density functional theory (DFT) calculations. The GGA-PBE functional was used for all computations, taking into account the exchange-correlation effects. The structural properties of Hf_2InN MAX phase were examined by calculating its ground-state energy, lattice parameters, and bond lengths between the atoms. The compound was found to have a minimum ground-state energy, which indicates that Hf_2InN is a structurally stable compound. The absence of negative frequency values in the phonon dispersion curve confirms that the material is dynamically stable. The value of the elastic constants, which satisfy Born's stability criteria, suggest that the compound is mechanically stable. Furthermore, the bond stretching, hardness, brittleness, and anisotropic nature are confirmed by the analysis of the material's mechanical parameters. The electronic band structure and density of states (DOS) plots were analyzed to study the electronic properties. These plots indicate that Hf_2InN exhibit metallic behavior. From the analysis of total density of states (TDOS) and partial density of states (PDOS) plots, the distributions of up- and down- spin states were found to be symmetric, confirming its non-magnetic nature. The optical properties of Hf_2InN are predicted through the analysis of its dielectric functions, refractive index, extinction coefficient, reflection coefficient, absorption coefficient, and energy loss function. The results show that the material exhibits strong light absorption, distinct energy loss peaks, high reflectivity, and significant optical anisotropy in the UV region, indicating its potential applications in optoelectronic devices, radiation shielding, UV absorption coating, and high temperature materials.

Keywords: Anisotropy, Band structure, DFT, Elastic constants, Moduli of rigidity

INTRODUCTION

The MAX phase compounds are ternary layered metal carbides or nitrides (Hadi et al., 2022). The general formula of MAX phase compound is $M_{n+1}AX_n$, where n = 1, 2, 3; M is an early transition metal, A is an element of group A, and X is carbon or nitrogen (Eklund et al., 2010; Hadi et al., 2022; Radovic & Barsoum, 2013a). The molecular structure of the MAX phase is defined by n, i.e., if n = 1, M_2AX [211], if n = 2, M_3AX_2 [312], and if n = 3, M_4AX_3 [413] (Eklund et al., 2010). Structurally, 2M layers are separated by a layer of A in [211], 3M layers by A in [312], and 4M layers by A in [413] (Eklund , 2010). The MAX phase compounds have hexagonal structure with space group $P6_3/mmc$ (Radovic & Barsoum, 2013a). In 1996, Barsoum and El-Raghy synthesized Ti_3SiC_2 compound which exhibited properties such as good thermal and electric conduction, readily mechanical, thermal shock resistance, plastic nature at high temperature, similar to metal, and properties such as corrosion resistance and heat tolerance, similar to ceramic (Barsoum & El-Raghy, 1996). This event opened the door for MAX phase as new field of research. These MAX phase compounds encompass the properties of metal and ceramic, so they are also known as metallic ceramic (Barsoum, 2000; Sun et al., 2006). MAX phases have nano-laminated structure with alternate metallic and ceramic layers (Radovic & Barsoum, 2013b). Due to strong M-X bond and weaker M-A bond, the MAX phase compounds get their unique properties (Eklund et al., 2010). These properties of MAX phase allow them to be used in various fields; such as high temperature coatings, electric contacts, nuclear industries and so on (Gonzalez-Julian, 2023). Nasir and team in 2014

investigated multiple physical properties of Zirconium-based MAX phases Zr_2AC (A = Al, Si, P and S) (Nasir et al., 2014). Filippatos et al., in 2019, studied elastic properties of various 312 MAX phase compounds using DFT method of calculations. In 2020, Ali et al. analyzed different physical properties of 212 MAX phase Ti_2InB_2, and compared it with the results of other similar 211 MAX phase (Ti_2InC, Ti_2SnC, Ti_2AlC) compounds (Ali et al., 2020). Yang and his co-workers in 2022, explored the phase stability, mechanical, and thermal properties of TM_3AlC_2 (TM = Ti, Zr and Hf) MAX phase compounds using DFT methods (Yang et al., 2022). In the year 2025, Oli and co-authors studied various fundamental physical properties of Ti_3GeC_2 and Ti_3SiC_2 MAX phase compounds using GGA: PBE and GGA: PBE+U functionals through DFT method of calculations (Oli et al., 2025). After reviewed the various literatures related to MAX phase compounds of their distinct physical properties and found that the structural, electronic, magnetic, optical, dynamical and mechanical properties of Hf_2InN MAX phase compound have not yet been studied. Therefore, our motivation goes to explore the structural, mechanical, dynamical, electronic, magnetic and optical properties of Hf_2InN MAX phase compound computationally using density functional theory (DFT) method of calculations employing quantum ESPRESSO as a computational tool.

MATERIALS AND METHODS

The structural, mechanical, dynamical, electronic, magnetic, and optical properties of Hf_2InN MAX phase compound were studied using Quantum ESPRESSO (QE) (Giannozzi et al., 2020) as computational tool. The plane-wave basis set, along with the projected Augmented wave (PAW) pseudopotential scheme, was used for the density functional theory (DFT) (Kohn & Sham, 1965; Hohenberg & Kohn, 1964) calculations. The exchange-correlation (XC) functional was treated using the generalized gradient approximation (GGA) with the Perdew-Burke-Ernzerhof (PBE) (Hammer et al., 1999) functional. The PBE has limited accuracy in describing electron correlation in transition metals like Hf, however the present results remain reliable for qualitative and comparative analysis. The cutoff energy of the plane-wave basis set was set to be 520 eV, and the energy convergence threshold was set to 10^{-7} eV to obtain the optimized structure. These values were obtained through the convergence test. The fully optimized and relaxed structure was achieved when the Hellmann-Feynman force (Feynman, 1939) on each atom became less than 0.01 eV/Å. The Brillouin zone was sampled using a set of special k-points generated by the Monkhorst-Pack scheme (Monkhorst & Pack, 1976). An (8×8×8) k-point mesh (estimated through the convergence test) was used for the self-consistent field (SCF) calculations. For the band structure calculations along high-symmetric paths, the same (8×8×8) k-point mesh in the irreducible Brillouin zone (BZ) was employed. However, a denser (16×16×16) k-point mesh was used in order to obtain smoother curves for the calculations of the density of states (DOS), and partial density of states (PDOS). Furthermore, the mechanical properties of the Hf_2InN MAX phase compound were estimated using the elastic constants (C_{ij}). For hexagonal structure, five independent elastic constants (C_{11}, C_{12}, C_{13}, C_{33}, and C_{44}) were calculated using stress-strain method (Chung & Buessem, 1967). These elastic constants were then used to evaluate the elastic moduli; namely bulk modulus (B), shear modulus (G), and Young's modulus (E), using the Vigot-Reuss-Hill approach (Chung & Buessem, 1967). With the help of these elastic moduli (B, G, and E), other mechanical properties such as Poisson's ratio (ν), Pugh's ratio (B/G), Cauchy pressure (P_C), the universal anisotropy index (A_U), Vicker's hardness coefficient (H_V), and Kleinman's parameter (ζ) were determined. The dynamical properties of the compound were studied by plotting the phonon dispersion curve (phonon frequency vs high symmetric points). This curve was obtained using density functional perturbation theory (DFPT) methods (Togo & Tanaka, 2015). To investigate the optical properties of the Hf_2InN MAX phase compound, the complex dielectric tensor $\varepsilon(\omega) = \varepsilon_1(\omega) + i\varepsilon_2(\omega)$, was calculated using ground-state DFT within random phase approximation (RPA) (Bohm & Pines, 1953; Körner & Elsässer, 2010). Using the complex dielectric function (real part $\varepsilon_1(\omega)$, and imaginary part $\varepsilon_2(\omega)$), the other optical properties, such as the refractive index, extinction coefficient, reflection coefficient (reflectivity), absorption coefficient, and energy loss function, were evaluated.

RESULTS AND DISCUSSION

Structural properties

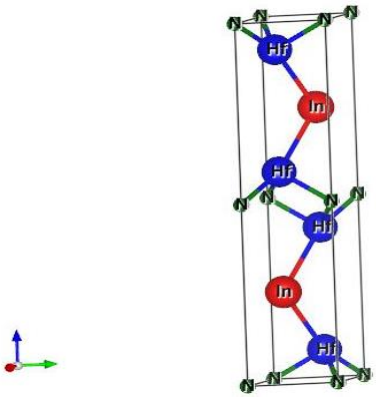

Figure 1. (Colour online) Unit structure of Hf_2InN Max phase compound, where blue, red, and green colour respectively represent Hf, In, and N, atom in the structure

Like all MAX phase materials, Hf_2InN crystalizes in a hexagonal structure with the space group $P6_3/mmc$ (Radovic & Barsoum, 2013a), and its unit cell contains eight atoms. First, we obtained the optimized and relaxed structure of Hf_2InN, which is shown in Figure 1. Then, for a detailed study of the structural properties, we examined various parameters such as lattice constants, bond lengths, and ground state energy based on the optimized structure. All these computational were performed using GGA: PBE functional in DFT methods of calculations. We calculated the lattice parameters (a = b, and c) and bond lengths of Hf_2InN before and after relaxation. The lattice constants before relaxation are found to be a = b = 3.29 Å and c = 15.05 Å, whereas after relaxation they became a = b = 3.32 Å and c = 14.88 Å. Similarly, the bond length of Hf-In, In-N, and Hf-N are 3.15 Å, 4.21 Å, and 2.27 Å, respectively before relaxation and 3.16 Å, 4.18 Å, and 2.26 Å, respectively after relaxation. The structural parameters (lattice constants and bond lengths) before and after relaxation are nearly identical. Table 1 summarizes the data of for both the unrelaxed and relaxed structures.

Table 1. Estimated structural parameters (lattice parameters and bond length) of Hf_2InN MAX phase compound before and after relaxation

	Lattice Parameters (Å)		**Bond Length (Å)**		
	a = b	c	Hf-In	In-N	Hf-N
Relaxation					
Before	3.29	15.05	3.15	4.21	2.27
After	3.32	14.48	3.16	4.18	2.26

Furthermore, we compared the lattice parameters of the relaxed Hf_2InN compound with the reported values for Ti_2InN and Hf_2AlN compounds, respectively (Uddin et al., 2022; Khediri et al., 2023). The structural parameters are found to be comparable with those reported in the literature. The comparative data are presented in Table 2.

Table 2. The calculated lattice parameters of the Hf_2InN compound are compared with the reported lattice parameters of Ti_2InN and Hf_2AlN compounds. All these calculations are performed using GGA: PBE functional

Materials	**Lattice Parameters (Å)**		**References**
	a = b	**c**	
Hf_2InN	3.32	14.48	Present work
Hf_2AlN	3.08	14.06	(Khediri et al., 2023)
Ti_2InN	3.25	14.29	(Uddin et al., 2022)

The calculated lattice parameters of Hf_2InN are in good agreement with the reported results of Khediri and his co-workers (Khediri et al., 2023) for Ti_2InN and Uddin and his co-authors (Uddin et al., 2022) for the Hf_2AlN compound. The ground-state energy and the binding energy of a material are inversely proportional to each other. In other words, a lower ground-state energy corresponds to a larger binding energy, and vice versa. A higher binding energy indicates that the atoms are more strongly bound to each other (Neupane & Adhikari, 2022). We calculated the ground-state energy of Hf_2InN using the PBE functional and found it to be -69.061 eV. This low ground-state energy reflects a high binding energy, indicating that the atoms are strongly bound. Hence, Hf_2InN is structurally stable.

Mechanical properties

The special properties (both ceramic and metallic) of MAX phase compounds are primarily reflected in their mechanical behavior. The mechanical properties of most MAX phase compounds depend on their grain size (Barsoum, 2000). These compounds, being layered solids, are intrinsically plastically anisotropic; that is, their mechanical properties are directional-dependent. Due to this plastic anisotropy, they lack the five independent slip systems necessary for ductility (Barsoum & Radovic, 2011). The elastic constants and moduli of elasticity govern the mechanical behavior

of solids. The elastic constants (C_{ij}) where i, j = 1, 2, 3, 4, 5, 6 can be used to evaluate the mechanical stability of a material. These constants reveal how materials respond to external stress or strain and provide insight into their bonding characteristics (Wang & Zhou, 2004). For hexagonal symmetry, there are five independent elastic constants. They are C_{11}, C_{12}, C_{13}, C_{33} and C_{44}. The elastic constants of the Hf_2InN MAX phase compound are calculated and are presented in Table 3. These computed values are comparable with the reported values of other similar MAX phase compounds.

Table 3. The estimated elastic constants (C_{ij}) of the Hf_2InN MaX phase compound (all values in GPa) are compared with the reported values of Ti_2InN and Hf_2AlN MAX phase compounds

C_{11}	C_{12}	C_{13}	C_{33}	C_{44}	References
279.81	76.08	64.81	246.38	73.55	Present work
247.26	66.53	91.79	242.20	94.62	(Khediri et al., 2023)
318.00	78.00	102.00	281.00	138.00	(Uddin et al., 2022)

Born's mechanical stability criteria are commonly employed to assess the stability of a material (Hadi et al., 2022). The Born stability criteria are (Born, 1940; Huang, 1996);

$$c_{11} > |c_{12}|;\ 2C_{13}^2 < C_{33}(C_{11} + C_{12});c_{44} > 0 \quad (1)$$

The estimated elastic constants of Hf_2InN satisfy the stability criteria (given in equation (1)); hence, the Hf_2InN is mechanically stable material. The moduli of elasticity (Young's modulus (E), shear modulus (G), and bulk modulus (B)) describe how solids respond to external forces such as compression, impact, and torsion. These elastic moduli are calculated using the Voigt (Voigt, 1889), Reuss (Reuss, 1929), and Hill (Hill, 1952) approximations. The bulk modulus (B) measures a material's resistance to change in volume without a change in shape. It is given by equations (2, 3, and 4) (Voigt, 1889; Reuss, 1929; Hill, 1952);

$$B_v = \frac{2(C_{11}+C_{12})+4C_{13}+C_{33}}{9} \quad (2)$$

$$B_R = \frac{(C_{11}+C_{12})C_{33}-2C_{12}^2}{C_{11}+C_{12}+2C_{33}-4C_{13}} \quad (3)$$

$$B_H = \frac{B_v+B_R}{2} \quad (4)$$

where, the subscripts V, R, and H stand for the Voigt, Reuss, and Hill approximations, respectively. The shear modulus (G) measures the rigidity of material. It is given by equations-(5, 6, and 7) for Voigt, Reuss, and Hill approximations (Hill, 1952; Reuss, 1929; Voigt, 1889);

$$G_v = \frac{C_{11}+C_{12}+2C_{33}-4C_{13}+12C_{44}+12C_{66}}{30} \quad (5)$$

$$G_R = \frac{\frac{5}{12}(C_{11}+C_{12})C_{33}-2C_{13}^2C_{44}C_{66}}{3B_vC_{44}C_{66}+\left((C_{11}+C_{12})C_{33}-2C_{13}^2\right)(C_{44}+C_{66})} \quad (6)$$

$$G_H = \frac{G_v+G_R}{2} \quad (7)$$

Young's modulus (E) measures the elasticity of material. It is calculated using equation (8) (Mo et al., 2014b);

$$E = \frac{9B_xG_x}{3B_x+G_x} \quad (8)$$

Here, the subscript x can be replaced by V, R or H. Poisson's ratio (ν) can be used to analyze the brittle or ductile nature of a material. If a material has a Poisson's ratio greater than 0.26, it exhibits ductile behavior; if the ratio is less than 0.26, it exhibits brittle behavior (Frantsevich, 1982). It is calculated using equation (9) (Mo et al., 2014a);

$$\nu = \frac{3B_xG_x}{2(3B_x+G_k)} \quad (9)$$

The elastic moduli (B, G, and E), and Poisson's ratio (ν) are calculated using the Voigt, Reuss, and Hill approximation. The calculated elastic moduli (B, G, and E) and Poisson's ratio (ν) are compared with the reported results and are listed in the Table 4.

Table 4. Elastic moduli (bulk modulus (B), shear modulus (G), and Young's modulus (E)) and Poisson's ratio (ν) of Hf_2InN compound, where moduli are measured in GPa. The subscripts R, V, and H refer to the Reuss, Voigt, and Hill approximation, respectively. The values are also compared with the reported values for the materials Ti_2InN and Hf_2AlN

B_R (GPa)	B_V (GPa)	B_H (GPa)	G_R (GPa)	G_V (GPa)	G_H (GPa)	E (GPa)	ν	References
134.51	135.27	134.89	87.62	89.81	88.71	218.29	0.23	Present work
137.23	137.44	137.33	87.39	88.36	87.88	217.29	0.23	(Khediri et al., 2023)
-	-	163.00	-	-	119.00	271.00	0.20	(Uddin et al., 2022)

The calculated values of the elastic moduli of Hf_2InN are found to be higher value. This value is also comparable to those of the similar material Ti_2InN (Khediri et al., 2023), and is slightly lower than those of Hf_2AlN (Uddin et al., 2022). This indicates that Hf_2InN provides strong resistance to compression and shape deformation. Since both Ti_2InN and Hf_2AlN exhibit strong bonding and require more energy to deform, Hf_2InN is also expected to possess bonding characteristics. Based on the calculated value of Young's modulus (E), Hf_2InN is found to be very stiff. We have found the value of Poisson's ratio (ν) of Hf_2InN to be 0.23, which is less than 0.26 (i.e. $\nu < 0.26$). Hence, the material exhibits a brittle nature. The brittleness of Hf_2InN can also be confirmed using Pugh's criterion. A material is considered brittle if B/G < 1.75 (Pugh, 1954). For Hf_2InN, B/G = 1.52, which is less than 1.75. These values are almost similar to the result obtained by Khediri et al. (2023). The nature of bonding at the atomic level is studied by analyzing the Cauchy pressure (P_C). For hexagonal crystal, it is given by (Jamal et al., 2014);

$$P_C = C_{12} - C_{44} \qquad (10)$$

If the Cauchy pressure (P_C) is positive, the bonding is metallic, whereas negative P_C signifies covalent bonding (Jamal et al., 2014). The Cauchy pressure (P_C) of Hf_2InN is found to be 2.5 GPa. The positive value of P_C suggests that the nature of bonding in the material is metallic. The anisotropic nature of Hf_2InN is predicted by calculating its Universal anisotropy index (A_U). The A_U is given by equation (11), (Ranganathan & Ostoja-Starzewski, 2008);

$$A_U = 5\left(\frac{G_V}{G_R}\right) + \left(\frac{B_V}{B_R}\right) - 6 \qquad (11)$$

where (G_V & G_R), and (B_V & B_R) represent the shear modulus and bulk modulus obtained from the Voigt and Reuss approximation, respectively. The value of the universal anisotropy index (A_U) for our material is found to be 0.13 (i.e., $A_U > 0$). Thus, the result suggests that Hf_2InN exhibits elastic anisotropy. We evaluated Vickers hardness (H_V) to study the hardness or softness of the material. The H_V is calculated using equation (12), (Tian et al., 2012);

$$H_v = 0.92\left(\frac{G}{B}\right)^{1.137} G^{0.708} \qquad (12)$$

The obtained value of Vickers hardness for Hf_2InN is 13.77 GPa, which suggests that the material is significantly hard. This value of H_V is in good agreement with the value (H_V = 13.17 GPa) of Ti_2InN material (Khediri et al., 2023). Furthermore, we studied the contribution of bond bending or stretching in resisting external pressure by evaluating Kleinman's parameter (ζ). It is given by equation (13), (Tian et al., 2012);

$$\zeta = \frac{2C_{11}+8C_{12}}{7C_{11}+2C_{12}} \qquad (13)$$

If $\zeta > 0.5$, the material exhibits bond stretching; otherwise of bond and otherwise, bond bending dominates (Kleinman, 1962). The calculated value of ζ for Hf_2InN is 0.55, indicates that bond stretching is dominant.

Dynamical properties

The dynamical stability of Hf_2InN was examined through its phonon dispersion curve. Figure 2 shows the phonon dispersion curve of Hf_2InN, where phonon frequency spectrum is plotted along high symmetry points, which are obtained using density functional perturbation theory (DFPT) (García & Vanderbilt, 1996; Togo & Tanaka, 2015). The dynamical stability of the material is determined by the phonon frequencies at the symmetric points. If the phonon frequency is positive at all high-symmetry points, the material is stable; Otherwise, it is unstable (García & Vanderbilt, 1996; Ali et al., 2016). In Figure 2, we observe that the phonon frequencies at every high-symmetry point are positive, indicating that Hf_2InN is dynamically stable. This means that the atomic arrangement of Hf_2InN can endure small lattice vibrations without spontaneously transforming into a new arrangement.

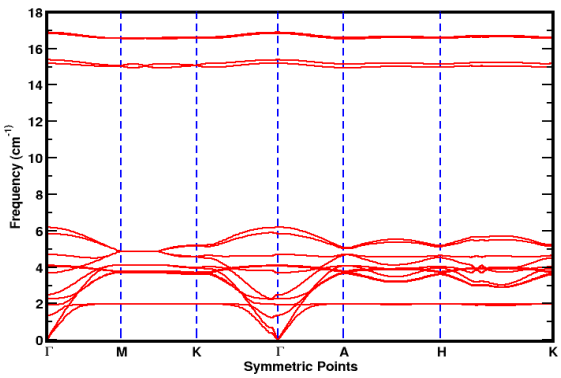

Figure 2. (Colour online) Phonon dispersion curve of Hf_2InN, where the high-symmetry points (Γ, M, K, Γ, A, H, K) are plotted on the X-axis, and corresponding phonon frequencies are plotted on the Y-axis. The blue vertical lines pass through the high-symmetry points

Moreover, we have discussed about the phonon frequency branches. There are two types of branches in the phonon dispersion curve. The lower branches are called acoustic branches, and upper branches are called optical branches. For every n atom in unit cell, it will have 3n vibrational branches. Among these branches, 3 are acoustic branches and 3n-3 are optical branches (Togo & Tanaka, 2015). As, Hf_2InN has 8 atoms in unit cell, it has 24 branches. Out of these, the lower 3 branches are acoustic branches and rest are

optical branches. The three acoustic branches arise as a result of in-phase movement of heavy (Hf and In) atoms. At the center of Brillouin Zone i.e., at Γ point, the frequency of all the acoustic branches is zero (i.e., $\omega = 0$ at Γ point). However, optical branches have non-zero frequency ($\omega \neq 0$) at Γ point. The optical branches are the resultant of out-of-phase movement of light (N) atom. The optical bands of Hf_2InN lies above the frequency of 2 cm^{-1}. These optical branches are responsible for optical behavior of material. Thus, we also study the optical behavior of the materials based on its phonon dispersion curve.

Electronic properties

The nature of a material (metallic, semiconducting, or insulating) can be determined from its electronic properties (Neupane & Adhikari, 2021). To investigate the electronic properties of Hf_2InN, we analyzed its band structure and density of states (DOS) plot. The calculated band structure of Hf_2InN is shown in Figure 3a, where the horizontal blue dashed line represents the Fermi energy level, set at 0 eV. This Fermi level acts as the boundary between the valence band and the conduction band. The valence band lies below the Fermi level, whereas conduction band lies above it. In Figure 3a, it is observed that the valence bands cross the Fermi level and overlap with the conduction bands. This overlap near the Fermi level eliminates the band gap, confirming the metallic nature of Hf_2InN. Therefore, Hf_2InN exhibits metallic behavior, providing evidence of its good electrical conductivity.

The density of states (DOS) describes the number of available energy states that electrons can occupy at a particular energy level. To investigate these available states, we constructed the DOS plot shown in Figure 3b. From the plot, we observe a non-zero (finite) density of states at the Fermi level. This indicates the presence of unoccupied energy states that electrons can occupy facilitating electron movement and electrical conduction. Therefore, the DOS plot further confirms that Hf_2InN exhibits metallic behavior.

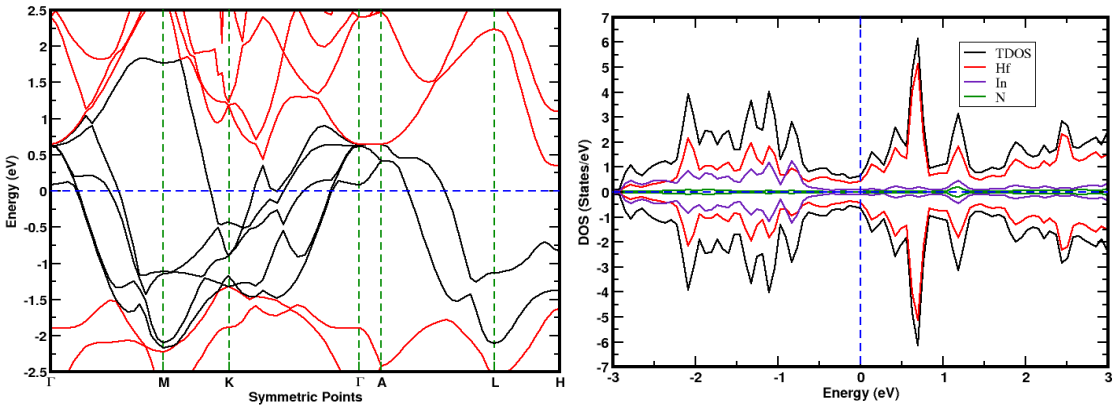

Figure 3. (Colour online) Band structure and density of states (DOS) plot of Hf_2InN; (a) band structure of Hf_2InN, where high-symmetry points are plotted in X-axis, their corresponding energy (eV) are taken in Y-axis, and blue horizontal line passing through 0 eV represents Fermi energy level, (b) DOS plot of Hf_2InN, where vertical blue dotted line represents Fermi energy level and horizontal blue dotted line separates up- and down-spin states

Magnetic properties

The magnetic properties of a material arise from the magnetic moment produced by unpaired up- and down-spins electrons in the atomic orbitals (Neupane & Adhikari, 2022; Paudel et al., 2023). To investigate the magnetic properties of Hf_2InN, we analyzed its total density of states (TDOS) and partial density of states (PDOS) plots. If the up- and down-spin states of electrons are asymmetrically distributed in the DOS and PDOS plots, the material exhibits magnetic behavior; otherwise, it is non-magnetic (Neupane et al., 2025a; Rijal et al., 2025). The TDOS and PDOS plots of Hf_2InN are shown in Figure 3b and Figure 4, respectively. In both plots, energy (eV) is represented on the X-axis, and the density of states (DOS) is represented on the Y-axis. In Figure 3b, the total density of states (TDOS), represented by the black line, is the result of the combination of the DOS of each atom; Hf, In, and N, which represented by red, purple, and green, respectively. In the TDOS plot, the up- and down-spin states of Hf_2InN near the Fermi level are distributed symmetrically. This symmetrical distribution of spin states indicates a zero magnetic moment, and therefore, Hf_2InN exhibits non-magnetic behavior. To examine the distribution of up- and down-spin electron states in detail, we analyzed the individual atomic orbitals using the PDOS plot, as shown in Figure 4.

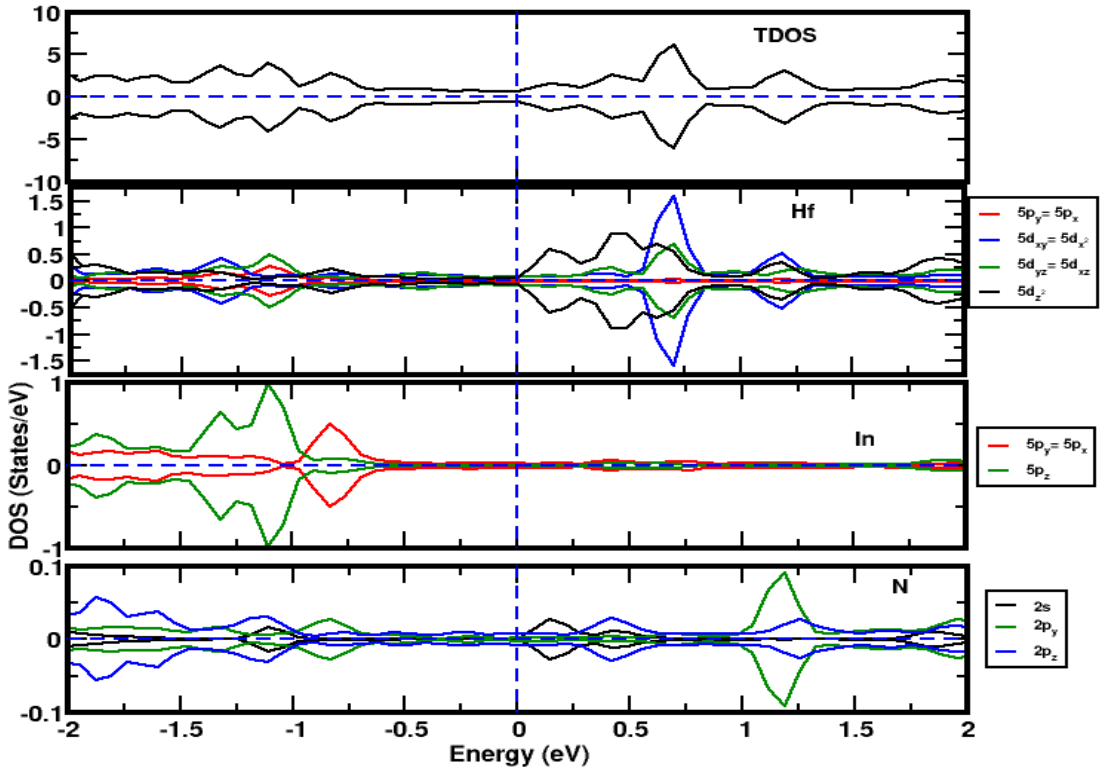

Figure 4. (Colour online) Partial density of states (PDOS) plot of Hf_2InN where vertical blue dotted line represents Fermi energy level and horizontal blue dotted line separates up- and down-spin states

From the PDOS plot, we can observe that the $5d_{xy}$, $5d_{xz}$, $5d_{yz}$, $5d_{x^2}$, and $5d_{z^2}$ orbitals are the dominant orbitals of the Hf atom. Among them, the $5d_{z^2}$ orbital contributes the highest magnetic moment of the Hf atom, with values of 0.22 μ_B/cell and -0.22 μ_B/cell for the up- and down-spin states, respectively. Similarly, all other orbitals of the Hf atom have equal values for the symmetrical up- and down-spin states, resulting in a net magnetic moment of zero for Hf. In the In atom, the $5p_y$ = $5p_x$, and $5p_z$ orbitals are dominant, with values 0.07 μ_B/cell and 0.11 μ_B/cell, respectively. These orbitals also exhibit symmetric up- and down-spin states. However, In has minimal contribution near the Fermi level and, therefore, does not contribute to the magnetic moment. For the N atom, the 2s, $2p_y$, and $2p_z$ orbitals near the Fermi level also display symmetric up-and down-spin distributions, resulting in zero magnetic moment. In conclusion, Hf_2InN exhibit non-magnetic behavior. The calculated magnetic moment arising from the up-and down-spin states of electrons in the individual orbitals of all atoms in the material are presented in Table 5.

Table 5. Magnetic moment (μ) calculated from the up- and down-spin states of electrons in the individual orbitals of N, Hf, and In atoms in the Hf_2InN MAX phase compound

Orbitals	μ of up-spin (μ_B/cell)	μ down-spin (μ_B/cell)	Resultant μ (μ_B/cell)
μ of 2s of N	0.0036	-0.0036	0.00
μ of $2p_y$ of N	0.0123	-0.0123	0.00
μ of $2p_z$ of N	0.0435	-0.0435	0.00
μ of $5p_x$ of Hf	0.0227	-0.0227	0.00
μ of $5d_{xy}$ of Hf	0.1935	-0.1935	0.00
μ of $5d_{z^2}$ of Hf	0.2209	-0.2209	0.00
μ of $5d_{xz}$ of Hf	0.1676	-0.1676	0.00
μ of $5p_z$ of In	0.1173	-0.1173	0.00
μ of $5p_x$ of In	0.0744	-0.0744	0.00
μ of $5p_{yz}$ of In	0.0098	-0.0098	0.00

Optical properties

he interaction of a material with electromagnetic (EM) radiation is determined by its optical properties. These optical properties are closely associated with the electronic structure of the material (Neupane et al., 2025b). We studied the variation in the optical properties of the material when an electric field (EM radiation) is applied in different directions. We plotted and analyzed dielectric function ε(ω), refractive index η(ω), extinction coefficient k(ω), absorption coefficient α(ω), reflection coefficient (reflectivity) R(ω), and energy loss function L(ω) of Hf_2InN to investigate its optical behavior. All these parameters are determined from the calculated real and imaginary parts of the dielectric function (Saeed et al., 2022), as given by equations-(14), (15), and (16), (Peter & Cardona, 2010);

$$\varepsilon(\omega) = \varepsilon_1(\omega) + i\varepsilon_2(\omega) \quad (14)$$

where $\varepsilon_1(\omega)$ is real part and $\varepsilon_2(\omega)$ is imaginary part of dielectric function. The imaginary part $\varepsilon_2(\omega)$ is directly computed from optical transitions using the formula (Adler, 1962; Yu & Cardona, 2010);

$$\varepsilon_2(\omega) = \frac{2e^2\pi}{\Omega\varepsilon_0}\sum_{k,v,c}|\langle\psi_k^c|u\cdot r|\psi_k^v\rangle|^2\delta(E_k^c - E_k^v - E) \quad (15)$$

The real part $\varepsilon_1(\omega)$ is derived from imaginary part $\varepsilon_2(\omega)$ by using the Kramers-Kronig relation (Adler, 1962);

$$\varepsilon_1(\omega) = 1 + \frac{2}{\pi}P\int_0^\infty \frac{\omega'\varepsilon_2(\omega')\,d\omega'}{\omega'^2-\omega^2} \quad (16)$$

where P denotes the principal value of the integral. The real part $\varepsilon_1(\omega)$ and imaginary part $\varepsilon_2(\omega)$ of the dielectric function of Hf_2InN are shown in Figure 5a and 5b, respectively.

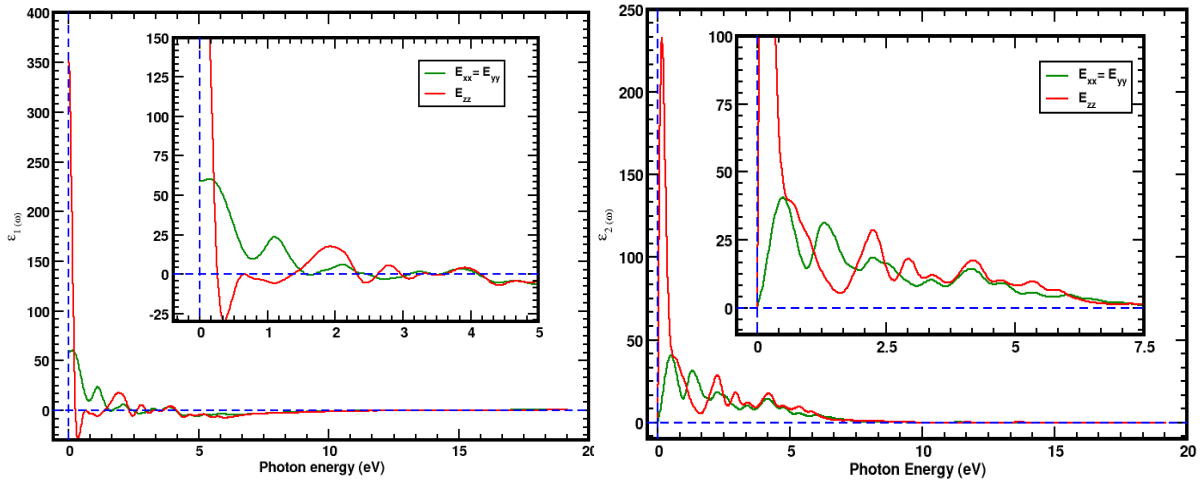

Figure 5. (Colour online) Variation of the dielectric function of Hf_2InN MAX phase compound; (a) variation of the real dielectric function with photon energy, and (b) variation of the imaginary dielectric function with photon energy. The insets represent the enlarged view of the real and imaginary parts of the dielectric function as a function of photon energy (eV) in each plot

In the plots, the photon energy (eV) is represented on the x-axis, and the dielectric functions are plotted on the y-axis. Both the real and imaginary parts of the dielectric function are analyzed over the photon energy range of (0-20) eV. The $\varepsilon_1(\omega)$ represents the strength of polarization (i.e., the ability to temporarily store electric energy) of the material. In the Figure 4a, the static dielectric constant $\varepsilon_1(0)$ for both the in-plane components ($\varepsilon_{xx} = \varepsilon_{yy} \approx 55$ eV) and out-of-plane component ($\varepsilon_{zz} \approx 350$ eV) exhibits large positive values. This suggests that Hf_2InN shows strong polarization (i.e., it can store energy in the form of electrostatic potential) and metallic character (Fig. 4b). The optical response of the material in the low-energy region (0-1) eV is attributed to intra-band transitions. The value of $\varepsilon_1(0)$ for the out-of-plane component (ε_{zz}) is significantly larger than that of the in-plane components ($\varepsilon_{xx} = \varepsilon_{yy}$), indicating that polarization along the c-axis is stronger than within the basal plane. This means the polarization along the c-axis is stronger than within the basal planes. Peaks observed in the energy range of (1-3) eV arise due to

inter-band transitions. The $\varepsilon_{xx} = \varepsilon_{yy}$ component becomes zero at approximately 1.7 eV photon energy, indicating the plasma frequency (ω_p). With a further increase in photon energy, $\varepsilon_1(\omega)$ becomes very small, suggesting that the material becomes less responsive to photons of that particular energy. The significant difference between the peak positions of the in-plane component ($\varepsilon_{xx}= \varepsilon_{yy}$) and out-of-plane ($\varepsilon_{zz}$) components confirms the intrinsic anisotropy of the material. Figure 5b represents the photon energy versus the imaginary part of the dielectric function $\varepsilon_2(\omega)$ of the Hf_2InN MAX phase material. $\varepsilon_2(\omega)$, measures photon absorption (i.e., how strongly photons are absorbed). The peak in $\varepsilon_2(\omega)$ indicate regions of strong optical absorption (Davies, 1954). In Figure 5b, both the in-plane components ($\varepsilon_{xx} = \varepsilon_{yy}$) and the out-of-plane component (ε_{zz}) exhibit large peak values near 0 eV. This indicates the absence of an optical band gap, suggesting that Hf_2InN is metallic in nature. The highest peak of $\varepsilon_2(\omega)$ is found to be approximately 230 at around 0.15 eV for the out-of-plane component (ε_{zz}). In contrast, for the in-plane components ($\varepsilon_{xx} = \varepsilon_{yy}$), the maximum value of $\varepsilon_2(\omega)$ is about 40 at approximately 0.7 eV photon energy. This suggests that the electronic transitions along the c-axis are stronger than those within the basal plane. Several peaks can be observed in the energy range of (0-5) eV, corresponding to interband transitions from the valence bands to the conduction bands. Furthermore, the value of $\varepsilon_2(\omega)$ drops to zero beyond 7.5 eV, indicating the cessation of interband transitions and the material becoming transparent in that energy region. The $\varepsilon_{xx} = \varepsilon_{yy}$ and ε_{zz} curves do not overlap, which indicates optical anisotropy in the material. The complex refractive index $\eta_c(\omega)$, which consists of a real part ($\eta(\omega)$) and an imaginary part ($k(\omega)$), describes the speed and bending behavior of light as it passes through a medium. It is given by equation-(17), (Ali et al., 2016; Ali et al., 2025);

$$\eta_c(\omega) = \eta(\omega) + ik(\omega) \quad (17)$$

The refractive index (real part) $\eta(\omega)$ is calculated using equation-(18), (Ali et al., 2025; Singh, 2006);

$$\eta(\omega) = \left(\frac{\sqrt{\varepsilon_1^2+\varepsilon_2^2}}{2} + \frac{\varepsilon_1}{2} \right)^{\frac{1}{2}} \quad (18)$$

And the extinction coefficient (imaginary part) $k(\omega)$ is estimated by equation (19), (Ali et al., 2025);

$$k(\omega) = \left(\frac{\sqrt{\varepsilon_1^2+\varepsilon_2^2}}{2} - \frac{\varepsilon_1}{2} \right)^{\frac{1}{2}} \quad (19)$$

The variation of refractive index and extinction coefficient with the photon energies are shown in Figures 6a and 6b, respectively.

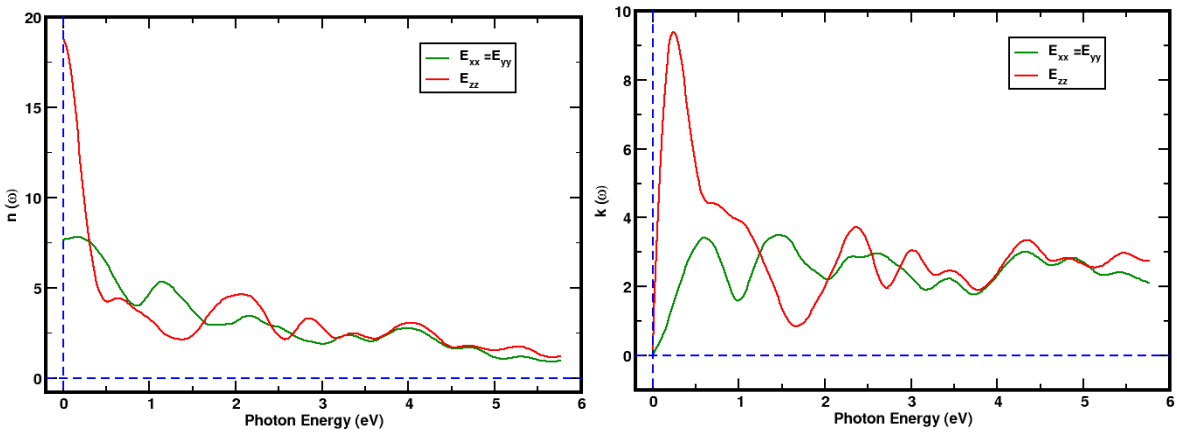

(a) **(b)**

Figure 6. (Colour online) The variation of refractive index and extinction coefficient of Hf_2InN MAX phase compound; (a) variation of refractive index with photon energy, and (b) variation of extinction coefficient with photon energy

The refractive index $\eta(\omega)$, is a dimensionless quantity that describes the path followed by light as it passes through a medium (Ali et al., 2016). In Figure 6a, which shows the refractive index plot, the value of the static refractive index $\eta(0)$, for both the in-plane ($\varepsilon_{xx} = \varepsilon_{yy}$) component and the out-of-plane (ε_{zz}) component is positive and large. This reflects the metallic nature of Hf_2InN. The peak value of $\eta(\omega)$ for $\varepsilon_{xx} = \varepsilon_{yy}$ and ε_{zz} are found to be approximately 7.52 and 18.7, respectively. These peak values for both components appear in the infrared (IR) region (0.00-1.60) eV. Therefore, Hf_2InN has potential applications in the field of infrared waveguides and photonic devices. The value of $\eta(\omega)$ gradually decreases with increasing photon energy. This suggests that high-energy photons (>6 eV) are refracted to a lesser extent by the material. The extinction coefficient $k(\omega)$ measures the amount of light absorbed per unit distance by the material (Ali

et al., 2016). The peak in k(ω) reflects strong absorption of light by the material. The value of k(ω) at 0 eV appears to be small, but both the in-plane and out-of-plane components increase very rapidly. This indicates the intra-band transitions, which are characteristic of metallic conductivity. The maximum value of k(ω) for the out-of-plane (ε_{zz}) component is 9.4, which occurs near 0.26 eV of photon energy. In contrast, the peak value for the in-plane ($\varepsilon_{xx} = \varepsilon_{yy}$) component, approximately 3.5, appears at around 1.5 eV. The higher value of the ε_{zz} component suggests stronger electronic transitions along the c-axis. Distinct peaks are observed between (1.5-3.0) eV (visible region), corresponding to inter-band transitions. Figure 6b) also indicates the optical anisotropy of Hf_2InN, as evidenced by the distinct curves of the $\varepsilon_{xx} = \varepsilon_{yy}$ and ε_{zz} components.

The variation of absorption coefficient α(ω) and energy loss function L(ω) with their corresponding photon energies are shown in Figure 7a and 7b, respectively.

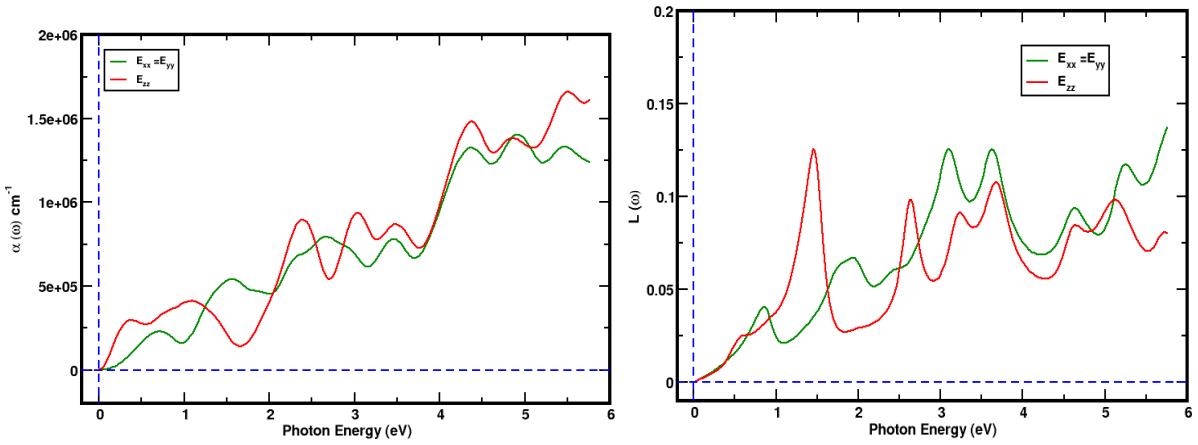

(a) **(b)**

Figure 7. (Colour online) Variation of the absorption coefficient and energy loss function with photon energies of Hf_2InN MAX phase compound; (a) absorption coefficient with photon energies of Hf_2InN, and (b) energy loss function with photon energies of Hf_2InN. The absorption coefficient and energy loss function of material are plotted along y-axis and corresponding photon energies are taken along x-axis

The α(ω) provides information about the penetration depth of light into a material at a specific frequency before being absorbed (Ali et al., 2016). It is calculated using the equation (20), (Ali et al., 2025);

$$\alpha(\omega) = \frac{2\omega}{c}\left(\frac{\sqrt{\varepsilon_1^2+\varepsilon_2^2}}{2} - \frac{\varepsilon_1}{2}\right)^{\frac{1}{2}} \qquad (20)$$

In Figure 7a, the peak of α(ω) indicates that light is efficiently absorbed at a particular photon energy. Two distinct curves are observed for the $\varepsilon_{xx} = \varepsilon_{yy}$ component and the ε_{zz} component, revealing the optical anisotropy of Hf_2InN. At low photon energies (< 1 eV), the value of α(ω) is small. It gradually increases with increasing photon energy, reaching a maximum of 1.41×10^6 at 4.91 eV for the $\varepsilon_{xx} = \varepsilon_{yy}$ component and 1.66×10^6 at 5.49 eV for the ε_{zz} component. Hence, strong light absorption occurs in the UV region, indicating that Hf_2InN can be used in UV mirror and optoelectronic devices.

In Figure 7b, the minimum value of L(ω) appears in the low energy (IR) region, indicating the absence of collective electrons excitations and suggesting the metallic nature of the material. However, a sharp peak for the out-of-plane (ε_{zz}) component is observed at around 1.5 eV of photon energy. The significant peaks for both the in-plane and out-of-plane components appear in the high-energy (UV) region. The ratio of the energy of the reflected wave to that of the incident wave striking the surface of a material is known as reflectivity (reflection coefficient) R(ω). Reflectivity provides information about the fraction of light reflected rather than absorbed. It is calculated using the relation (22), (Ali et al., 2025);

The energy loss function L(ω), represents the amount of energy lost by a fast electron as it travels through the material. L(ω) indicates energy loss due to the collective oscillation of electron (Ali et al., 2016). The energy loss function is calculated using equation (21), (Ali et al., 2025);

$$L(\omega) = \frac{\varepsilon_2}{\varepsilon_1^2+\varepsilon_2^2} \qquad (21)$$

$$R(\omega) = \frac{(n-1)^2+k^2}{(n+1)^2+k^2} \quad (22)$$

The variation of reflectivity of Hf_2InN with its corresponding photon energy is shown in Figure 8.

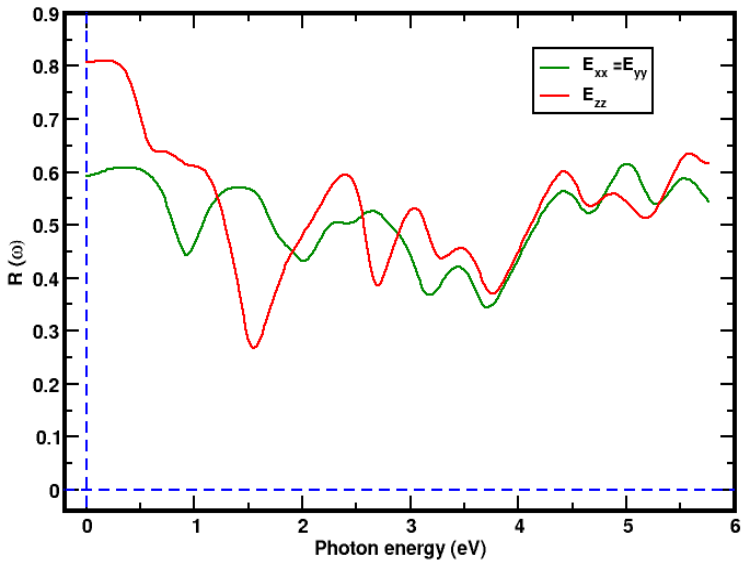

Figure 8. (Colour online) Variation of the reflection coefficient (reflectivity) of Hf_2InN with photon energy, where photon energy (eV) is plotted on the x-axis and reflectivity R(ω) is plotted on the y-axis

The value of static reflectivity (reflectivity at 0 eV), R(0), is high for both components. For the in-plane ($\varepsilon_{xx} = \varepsilon_{yy}$) component, R(0) is about 0.6 (60% reflection), while for the out-of-plane (ε_{zz}) component, it is about 0.8 (80% reflection, 20% absorption). This indicates a large presence of free electrons, suggesting that the material exhibits metallic character. In the energy range (2.00-5.00) eV, multiple peaks in R(ω) are observed, corresponding to inter-band transitions. The ε_{zz} curve is consistently higher than the $\varepsilon_{xx} = \varepsilon_{yy}$ curve, indicating stronger reflection perpendicular to the basal plane. The distinct curves of $\varepsilon_{xx} = \varepsilon_{yy}$ and ε_{zz} components reveal that the material exhibits anisotropic reflectivity.

CONCLUSION

We investigated the structural, mechanical, dynamical, electronic, magnetic, and optical properties of the Hf_2InN MAX phase compound. The calculations are performed using first principles methods based on density functional theory (DFT). The exchange-correlational interactions are computed using GGA: PBE functional, and Quantum ESPRESSO (QE) is employed as the computational tool. We first optimized the unit cell structure and then calculated the lattice parameters, bond lengths, and ground-state energy. The results are evaluated and compared with previously reported data, indicating that the material is structurally stable. The mechanical properties of the material are studied by analyzing parameters such as moduli of rigidity (B, G and E), Poisson's ration (v), Pugh's ratio (B/G), Cauchy Pressure (Pc), Kleinman's parameter (ζ), Vickers hardness (H_V), and Universal elastic anisotropy (A_U). These parameters are determined using elastic constants C_{ij} of Hf_2InN. The Hf_2InN satisfies the mechanical stability criteria, indicating that the material is mechanically stable. The Poisson's ratio and Pugh's ratio suggest that the material exhibits a brittle nature. Similarly, we found that Hf_2InN exhibits metallic bonding, as indicated by the Cauchy Pressure, and resists external pressure through bond stretching, as indicated by the Kleinman's parameter (ζ). The Vickers hardness and universal elastic anisotropy confirm that Hf_2InN is significantly hard and exhibits elastic anisotropy, respectively. Furthermore, the phonon frequency curve verifies the material's dynamical stability. The energy band plot and density of states (DOS) reveal the metallic nature of the material. The total DOS (TDOS) plot shows that the up- and down-spin states are symmetrically distributed at the Fermi energy level, indicating that the material is non-magnetic. This result is further supported by the partial DOS (PDOS) plot. The optical properties, including the dielectric functions, refractive index, extinction coefficient, absorption coefficient, energy loss function, and reflectivity, are studied in detail. The study revealed that the material exhibit strong light absorption in the UV region, distinct energy loss peaks, and high reflectivity. Hf_2InN also shows pronounced optical anisotropy, as

the curves of the in-plane ($\varepsilon_{xx} = \varepsilon_{yy}$) and out-of-plane ($\varepsilon_{zz}$) components do not overlap. Overall, Hf_2InN is structurally, mechanically, and dynamically stable, with potential applications in optoelectronic devices, UV mirrors, and high-temperature materials.

ACKNOWLEDGMENTS

The authors would like to thank the condensed matter research lab CDP TU, TWAS research funds for the computing capacity, and Prof. N. P. Adhikari for his constructive suggestions on the manuscript.

AUTHORS CONTRIBUTION

Conceptualization: SS and HKN; Methodology: SS, BD, ST, DD, GP, and OSR; Data analysis: HKN, SS; Writing-original draft: SS; Writing-review & editing: HKN, SS Supervision: HKN

FUNDING

TWAS research funds RG 20-316, Network project NT-14 of ICTP/OE

ORCIDs

Sushil Shrestha:
https://orcid.org/0009-0002-0656-6016
Suraj Timalsina:
https://orcid.org/0009-0007-7049-5693
Bibek Dhital:
https://orcid.org/0009-0007-4702-6063
Dipesh Dhital:
https://orcid.org/0009-0008-5512-244X
Ganesh Paudel:
https://orcid.org/0009-0007-0687-7486
Om Shree Rijal:
https://orcid.org/0009-0007-3646-173X
Hari Krishna Neupane:
https://orcid.org/0000-0001-8547-1183

CONFLICT OF INTEREST

The authors declare that there are no conflicts of interest regarding the publication of this article.

ETHICAL STATEMENT

The authors declare that it is their original work and has not been previously published or submitted for publication elsewhere.

DATA AVAILABILITY STATEMENT

The data supporting the findings of this study are available from the corresponding author upon reasonable request.

REFERENCES

Adler, S. L. (1962). Quantum Theory of the Dielectric Constant in Real Solids. *Physical Review*, *126*(2), 413–420. https://doi.org/10.1103/PhysRev.126.413

Ali, M. A., Nasir, M. T., Khatun, M. R., Islam, A. K. M. A., & Naqib, S. H. (2016). An *ab initio* investigation of vibrational, thermodynamic, and optical properties of Sc_2AlC MAX compound. *Chinese Physics B*, *25*(10), 103102. https://doi.org/10.1088/1674-1056/25/10/103102

Ali, M., Bibi, Z., Kanwal, S., Fatima, T., Raheel, M., Khan, A. F., & Kaleem, M. (2025). A comprehensive investigation of structural, mechanical and optoelectronics attributes of M_2AsC (M= Zr, Hf, Ta, W) MAX phase carbides: A DFT investigation. *Journal of Molecular Graphics and Modelling*, *140*, 109102. https://doi.org/10.1016/j.jmgm.2025.109102

Ali, M. M., Hadi, M. A., Ahmed, I., Haider, A., & Islam, A. (2020). Physical properties of a novel boron-based ternary compound Ti2InB2. *Materials Today Communications*, *25*, 101600. https://doi.org/10.1016/j.mtcomm.2020.101600

Barsoum, M. W. (2000). The MN+ 1AXN phases: A new class of solids: Thermodynamically stable nanolaminates. *Progress in Solid State Chemistry*, *28*(1–4), 201–281. https://doi.org/10.1016/S0079-6786(00)00006-6

Barsoum, M. W., & El-Raghy, T. (1996). Synthesis and characterization of a remarkable ceramic: Ti3SiC2. *Journal of the American Ceramic Society*, *79*(7), 1953–1956. https://doi.org/10.1111/j.11512916.1996.tb08018.x

Barsoum, M. W., & Radovic, M. (2011). Elastic and Mechanical Properties of the MAX Phases. *Annual Review of Materials Research*, *41*(1), 195–227. https://doi.org/10.1146/annurev-matsci-062910-100448

Bohm, D., & Pines, D. (1953). A Collective Description of Electron Interactions: III. Coulomb Interactions in a Degenerate Electron Gas. *Physical Review*, *92*(3), 609–625. https://doi.org/10.1103/PhysRev.92.609

Born, M., & Huang, K. (1996). *Dynamical Theory of Crystal Lattices*. Oxford University PressNew York, NY. https://doi.org/10.1093/oso/9780192670083.001.0001

Chung, D. H., & Buessem, W. R. (1967). The Voigt-Reuss-Hill Approximation and Elastic Moduli of Polycrystalline MgO, CaF2, β-ZnS, ZnSe, and CdTe. *Journal of AppliedPhysics*, *38*(6), 2535–2540.https://doi.org/10.1063/1.1709944

Davies, M. (1954). Dielectric absorption. *Quarterly Reviews, Chemical Society*, *8*(3), 250. https://doi.org/10.1039/qr9540800250

Eklund, P., Beckers, M., Jansson, U., Högberg, H., & Hultman, L. (2010). The Mn+ 1AXn phases: Materials science and thin-film processing. *Thin*

Solid Films, *518*(8), 1851–1878. https://doi.org/10.1016/j.tsf.2009.07.184

Feynman, R. P. (1939). Forces in molecules. *Physical Review*, *56*(4), 340. https://doi.org/10.1103/PhysRev.56.340

Filippatos, P. P., Hadi, M. A., Christopoulos, S.-R., Kordatos, A., Kelaidis, N., Fitzpatrick, M. E., Vasilopoulou, M., & Chroneos, A. (2019). 312 MAX phases: Elastic properties and lithiation. *Materials*, *12*(24), 4098. https://doi.org/10.3390/ma12244098

García, A., & Vanderbilt, D. (1996). First-principles study of stability and vibrational properties of tetragonal PbTiO3. *Physical Review B*, *54*(6), 3817–3824. https://doi.org/10.1103/PhysRevB.54.3817

Giannozzi, P., Baseggio, O., Bonfà, P., Brunato, D., Car, R., Carnimeo, I., Cavazzoni, C., De Gironcoli, S., Delugas, P., & Ferrari Ruffino, F. (2020). Quantum ESPRESSO toward the exascale. *The Journal of Chemical Physics*, *152*(15). https://doi.org/10.1063/5.0005082

Gonzalez-Julian, J. (2023). MAX phases: From synthesis to applications. *98th DKG Annual Meeting*.

Hadi, M. A., Christopoulos, S.-R. G., Chroneos, A., Naqib, S. H., & Islam, A. K. M. A. (2022). DFT insights into the electronic structure, mechanical behaviour, lattice dynamics and defect processes in the first Sc-based MAX phase Sc2SnC. *Scientific Reports*, *12*(1), 14037. https://doi.org/10.1038/s41598-022-18336-z

Hadi, M., Kelaidis, N., Filippatos, P.-P., Christopoulos, S.-R., Chroneos, A., Naqib, S., & Islam, A. (2022). Optical response, lithiation and charge transfer in Sn-based 211 MAX phases with electron localization function. *Journal of Materials Research and Technology*, *18*, 2470–2479. https://doi.org/10.1016/j.jmrt.2022.03.083

Hammer, B., Hansen, L. B., & Nørskov, J. K. (1999). Improved adsorption energetics within density-functional theory using revised Perdew-Burke-Ernzerhof functionals. *Physical Review B*, *59*(11), 7413. https://doi.org/10.1103/PhysRevB.59.7413

Hill, R. (1952). The Elastic Behaviour of a Crystalline Aggregate. *Proceedings of the Physical Society. Section A*, *65*(5), 349–354. https://doi.org/10.1088/0370-1298/65/5/307

Hohenberg, P., & Kohn, W. (1964). Inhomogeneous electron gas. *Physical Review*, *136*(3B), B864. DOI: https://doi.org/10.1103/PhysRev.136.B864

Jamal, M., Sarvestani, N. K., Yazdani, A., & Reshak, A. H. (2014). Mechanical and thermodynamically properties of hexagonal compounds at optimized lattice parameters from two-dimensional search of the equation of state. *RSC Advances*, *4*(101), 57903-57915. https://doi.org/10.1039/C4RA09358E

Khediri, R., Hammoutène, D., Kassali, K., Rodríguez-Hernández, P., & Muñoz, A. (2023). High-pressure structural, elastic, vibrational, and thermodynamic study of MAX-phase Ti2InN. *Computational Condensed Matter*, *36*, e00829. https://doi.org/10.1016/j.cocom.2023.e00829

Kleinman, L. (1962). Deformation Potentials in Silicon. I. Uniaxial Strain. *Physical Review*, *128*(6), 2614–2621. https://doi.org/10.1103/PhysRev.128.2614

Kohn, W., & Sham, L. J. (1965). Self-consistent equations including exchange and correlation effects. *Physical Review*, *140*(4A), A1133. DOI: https://doi.org/10.1103/PhysRev.140.A1133

Körner, W., & Elsässer, C. (2010). First-principles density functional study of dopant elements at grain boundaries in ZnO. *Physical Review B*, *81*(8), 085324. https://doi.org/10.1103/PhysRevB.81.085324

Mo, Y., Aryal, S., Rulis, P., & Ching, W. (2014a). Crystal Structure and Elastic Properties of Hypothesized MAX Phase-Like Compound $(Cr_2Hf)_2$ Al_3C_3. *Journal of the American Ceramic Society*, *97*(8), 2646–2653. https://doi.org/10.1111/jace.12987

Mo, Y., Aryal, S., Rulis, P., & Ching, W. (2014b). Crystal Structure and Elastic Properties of Hypothesized MAX Phase-Like Compound (Cr 2 Hf) 2 Al 3 C 3. *Journal of the American Ceramic Society*, *97*(8), 2646–2653. https://doi.org/10.1111/jace.12987

Monkhorst, H. J., & Pack, J. D. (1976). Special points for Brillouin-zone integrations. *Physical Review B*, *13*(12), 5188. https://doi.org/10.1103/PhysRevB.13.5188

Nasir, M. T., Hadi, M. A., Naqib, S. H., Parvin, F., Islam, A., Roknuzzaman, M., & Ali, M. S. (2014). Zirconium metal-based MAX phases Zr 2 AC (A= Al, Si, P and S): A first-principles study. *International Journal of Modern Physics B*, *28*(32), 1550022. https://doi.org/10.1142/S0217979215500228

Neupane, H. K., & Adhikari, N. P. (2021). Electronic and magnetic properties of defected MoS2 monolayer. *BIBECHANA*, *18*(2), 68–79. https://doi.org/10.3126/bibechana.v18i2.33905

Neupane, H. K., & Adhikari, N. P. (2022). Adsorption of water on C sites vacancy defected graphene/h-BN: First-principles study. *Journal of Molecular Modeling*, *28*(4), 107. https://doi.org/10.1007/s00894-022-05101-2

Neupane, H. K., Oli, D., Rijal, O. S., Neupane, R. K., Shrestha, P., Sharma, S., Joshi, L. P., & Parajuli, R. (2025a). Exploring the structural, dynamical, mechanical, electronic, magnetic, and optical

properties of Ta2AlN, Ti2AlN & Ti2GaN MAX phase compounds: First-principles study. *Heliyon*, *11*(6). https://www.cell.com/heliyon/fulltext/S2405-8440(25)01343-X

Neupane, H. K., Rijal, O. S., Neupane, R. K., Paudel, G., Shrestha, P., Sharma, S., Joshi, L. P., & Parajuli, R. (2025b). Structural, dynamical, thermomechanical, electronic, magnetic, and optical properties of M_2 AC (M = Ta, Sc; A = Al, Cd) MAX phase compound Via DFT approach. *Physica Scripta*, *100*(9), 095921. https://doi.org/10.1088/1402-4896/adffc6

Oli, D., Neupane, H. K., Neupane, R. K., Rijal, O. S., Shrestha, P., Sharma, S., Joshi, L. P., & Parajuli, R. (2025). Comprehensive study of structural, mechanical, dynamical, electronic, magnetic, and optical properties of Ti3GeC2 and Ti3SiC2 compounds via DFT approach. *Physica B: Condensed Matter*, *702*, 417009. https://doi.org/10.1016/j.physb.2025.417009

Paudel, G., Nepal, M., Aryal, S., Devkota, A., & Neupane, H. K. (2023). Effect of Water Adsorption on Bilayer h-BN: First-Principles Study. *Journal of Nepal Physical Society*, *9*(2), 56–62. https://doi.org/10.3126/jnphyssoc.v9i2.62323

Pugh, S. F. (1954). XCII. Relations between the elastic moduli and the plastic properties of polycrystalline pure metals. *The London, Edinburgh, and Dublin Philosophical Magazine and Journal of Science*, *45*(367), 823–843. https://doi.org/10.1080/14786440808520496

Radovic, M., & Barsoum, M. W. (2013a). MAX phases: Bridging the gap between metals and ceramics. *American Ceramics Society Bulletin*, *92*(3), 20–27.

Radovic, M., & Barsoum, M. W. (2013b). MAX phases: Bridging the gap between metals and ceramics. *American Ceramics Society Bulletin*, *92*(3), 20–27.

Ranganathan, S. I., & Ostoja-Starzewski, M. (2008). Universal Elastic Anisotropy Index. *Physical Review Letters*, *101*(5), 055504. https://doi.org/10.1103/PhysRevLett.101.055504

Reuss, A. (1929). Berechnung der Fließgrenze von Mischkristallen auf Grund der Plastizitätsbedingung für Einkristalle . *ZAMM - Journal of Applied Mathematics and Mechanics / Zeitschrift Für Angewandte Mathematik Und Mechanik*, *9*(1), 49–58. https://doi.org/10.1002/zamm.19290090104

Rijal, O. S., Neupane, H. K., Poudel, G., Yadav, S. K., & Parajuli, R. (2025). Mechanical, dynamical, thermal, electronic, magnetic and optical properties of XFeSb (X = Nb, V, Ta) half-heusler compounds: First-principles study. *Himalayan Physics*, *12*, 83–100. https://doi.org/10.3126/hp.v12i1.85760

Saeed, A., Adewuyi, S. O., Ahmed, H. A. M., Alharbi, S. R., Al Garni, S. E., & Abolaban, F. (2022). Electrical and Dielectric Properties of the Natural Calcite and Quartz. *Silicon*, *14*(10), 5265–5276. https://doi.org/10.1007/s12633-021-01318-7

Sun, Z. M., Hashimoto, H., Zhang, Z. F., Yang, S. L., & Tada, S. (2006). Synthesis and characterization of a metallic ceramic material–Ti3SiC2. *Materials Transactions*, *47*(1), 170–174. https://doi.org/10.2320/matertrans.47.170

Tian, Y., Xu, B., & Zhao, Z. (2012). Microscopic theory of hardness and design of novel superhard crystals. *International Journal of Refractory Metals and Hard Materials*, *33*, 93–106. https://doi.org/10.1016/j.ijrmhm.2012.02.021

Timsina, S., Dhital, B., Shrestha, S., Dhital, D., Paudel, G., Rijal, O. S., & Neupane, H. K. (2025). First-principles Insights Into the Structural, Mechanical, Optical, Magnetic, Electronic, and Dynamical Properties of Hf_2CdN MAX phase Compound. *Api Journal of Science*, *2*, 54–64. https://doi.org/10.3126/ajs.v2i1.87758

Togo, A., & Tanaka, I. (2015). First principles phonon calculations in materials science. *Scripta Materialia*, *108*, 1–5. https://doi.org/10.1016/j.scriptamat.2015.07.021

Uddin, M. M., Ali, M. A., Hossain, M. M., Naqib, S. H., & Islam, A. K. M. A. (2022). Comparative study of predicted MAX phase Hf2AlN with recently synthesized Hf2AlC: A first principle calculations. *Indian Journal of Physics*, *96*(5), 1321–1333. https://doi.org/10.1007/s12648-021-02050-z

Voigt, W. (1889). Ueber die Beziehung zwischen den beiden Elasticitäts constanten isotroper Körper. *Annalen Der Physik*, *274*(12), 573–587. https://doi.org/10.1002/andp.18892741206

Wang, J., & Zhou, Y. (2004). Dependence of elastic stiffness on electronic band structure of nanolaminate M2AlC (M = Ti, V, Nb, and Cr) ceramics. *Physical Review B*, *69*(21), 214111. https://doi.org/10.1103/PhysRevB.69.214111

Yang, A., Duan, Y., Bao, L., Peng, M., & Shen, L. (2022). Elastic properties, tensile strength, damage tolerance, electronic and thermal properties of TM3AlC2 (TM= Ti, Zr and Hf) MAX phases: A first-principles study. *Vacuum*, *206*, 111497. https://doi.org/10.1016/j.vacuum.2022.111497Get rights and content

Yu, P. Y., & Cardona, M. (2010). *Fundamentals of Semiconductors: Physics and Materials Properties*. Springer Berlin Heidelberg. https://doi.org/10.1007/978-3-642-00710-1